The global hydroclimate response during the Younger Dryas event

Renssen, Hans; Goosse, Hugues; Roche, Didier M.; Seppä, Heikki

published in
Quaternary Science Reviews
2018

DOI (link to publisher)
10.1016/j.quascirev.2018.05.033

document version
Publisher's PDF, also known as Version of record

Quaternary Science Reviews 193 (2018) 84–97

Contents lists available at ScienceDirect

Quaternary Science Reviews

journal homepage: www.elsevier.com/locate/quascirev

The global hydroclimate response during the Younger Dryas event

Hans Renssen [a, b, *], Hugues Goosse [c], Didier M. Roche [b, d], Heikki Seppä [e]

[a] Department of Natural Sciences and Environmental Health, University of South-Eastern Norway, N-3800, Bø i Telemark, Norway
[b] Department of Earth Sciences, VU University Amsterdam, NL-1081HV, Amsterdam, The Netherlands
[c] Earth and Life Institute, Georges Lemaître Centre for Earth and Climate Research, Université catholique de Louvain, B-1348, Louvain-la-Neuve, Belgium
[d] Laboratoire des Sciences du Climat et de l'Environnement (LSCE), CEA/CNRS-INSU/UVSQ, F-91191, Gif-sur-Yvette Cedex, France
[e] Department of Geosciences and Geography, University of Helsinki, P.O.BOX 64, FI-00014, Helsinki, Finland

ARTICLE INFO

Article history:
Received 25 January 2018
Received in revised form
9 May 2018
Accepted 24 May 2018
Available online 20 June 2018

Keywords:
Paleoclimate modelling
Global
Younger Dryas

ABSTRACT

To analyze the global hydroclimate response during the Younger Dryas cold event, we evaluate climate model results that have been constrained with proxy-based temperatures from the North Atlantic region. We find that both the temperature and the hydroclimate response have a clear global signature. A marked cooling is simulated over the North Atlantic Ocean (more than 5 °C) and the downwind continents (2–4 °C). This response is related to the weakening of the Atlantic meridional overturning circulation under influence of meltwater discharges. The hydroclimate response is most expressed over Eurasia in a belt between 40 and 60°N, and over Northern Africa in the Sahel region. In both areas, a strong decrease in soil moisture is simulated (up to 20% reduction). In contrast, a striking increase in moisture is found over southeastern North America (15% increase), where southerly atmospheric flow brings moist air to the continent. Outside these areas that are clearly affected by the cold North Atlantic Ocean, the responses of temperature and moisture are decoupled, with different causes for these temperature and hydroclimate responses. In the tropics, the hydroclimate response is governed by the southward shift of the intertropical convergence zone (ITCZ) due to the cooling of the North Atlantic Ocean. This causes drier conditions north of the equator and wetter conditions in the Southern Hemisphere tropics. The associated changes in soil moisture are relatively gradual here, taking up to two centuries to complete, suggesting that the impact of the ITCZ shift on the tropical hydroclimate is building up. Our experiment indicates that Southern Hemisphere continents experienced a small cooling (less than 0.5 °C) during the Younger Dryas, caused by the negative radiative forcing associated with reduced atmospheric methane concentrations and enhanced dust levels. In our simulation, the bi-polar seesaw mechanism is relatively weak, so that the associated warming of the South Atlantic Ocean is not overwhelming the reduction in radiative forcing. Our results thus indicate that in the tropics and/or Southern Hemisphere, the cooling is a response to the negative radiative forcing, while the hydroclimatic changes are predominantly resulting from ITCZ variations. Consequently, when interpreting hydroclimatic proxy records from these regions, data should not be compared directly to key records from high latitudes, such as Greenland ice core stable isotope records.

1. Introduction

The Younger Dryas (YD) is a prominent climate cooling event that interrupted the deglacial warming trend in the Northern Hemisphere between 12.9 and 11.7 thousand calendar years ago (Rasmussen et al., 2006; Carlson, 2013). The YD has been widely studied as an example of abrupt climate change, both using proxy-based reconstructions (e.g., Shakun and Carlson, 2010; Heiri et al., 2014) and numerical climate models (e.g., Manabe and Stouffer, 1997; He et al., 2013; Renssen et al., 2015). The focus in these modelling studies has been mainly on the temperature response, showing strongest cooling in the North Atlantic region, associated with a reduced strength of the Atlantic Meridional Overturning Circulation (AMOC). The hydroclimatic response is less clear, with a relatively complex spatial structure deduced from available proxy-based analyses. For instance, as reviewed by Carlson (2013),

* Corresponding author. Department of Natural Sciences and Environmental Health, University of South-Eastern Norway, N-3800, Bø i Telemark, Norway.
E-mail address: hans.renssen@usn.no (H. Renssen).

https://doi.org/10.1016/j.quascirev.2018.05.033
0277-3791/

reconstructions in North America suggest that the climate was drier in maritime Canada and the north-central United States (e.g., Dorale et al., 2010), while it was markedly wetter in the southeastern and southwestern United States (e.g., Polyak et al., 2004; Grimm et al., 2006).

The large-scale hydroclimate response during the Younger Dryas has been addressed in relatively few modelling studies. Recently, Jomelli et al. (2014) compared glacier extent records in the Andes with the response in a transient climate simulation performed with the CCSM3 model by He et al. (2013). Comparing the simulated YD response at 12 ka with the period just before at 12.9 ka, they found a latitudinal band with a marked decrease in precipitation stretching from the eastern equatorial Pacific Ocean, Central America and the northern Andean basin, to the equatorial North Atlantic Ocean and Western Africa. In contrast, a clear increase in precipitation was simulated south of the equator over the tropical South Atlantic and South Pacific Oceans. A weaker version of this contrasting pattern north and south of the equator was found further east over the Indian Ocean and the Indonesian Archipelago. In the CCSM3 model, this contrast in precipitation response is linked to the strong reduction in AMOC strength during the YD, and the associated temperature pattern showing marked cooling in the North Atlantic and warming in the South Atlantic (Jomelli et al., 2014). This temperature pattern leads to a mean southward shift of the ITCZ, resulting in a wetter climate south of the equator, but drying in the area to the north. This effect is especially strong over the tropical Atlantic, but the ITCZ also moves southward over the Indian Ocean (Mohtadi et al., 2014) and the tropical Pacific Ocean (Jomelli et al., 2014). A similar tropical response has been found in more idealized experiments with a suit of models in which the AMOC was perturbed using a freshwater 'hosing' in the North Atlantic (Stouffer et al., 2006).

Most YD modelling studies so far focused on the impact of an AMOC weakening, but did not address the impact of other forcings that were also important during YD time, such as the reduction in radiative forcing related to the drop in atmospheric methane levels. In addition, it is not clear from these studies how the temporal variability in the hydroclimate response compared to the temperature response. A recent overview of proxy-based reconstructions from Southeast Asia indicates that the hydroclimate response was much more gradual there than the abrupt temperature response in the North Atlantic region (Partin et al., 2015). This suggests that the spatio-temporal variability in the response in temperature and precipitation is complex. To address this variability, and specifically the impact of other forcings, we perform an analysis of transient simulations of the global YD climate.

In the present study, we analyze the temporal and spatial hydroclimate response during the YD in transient climate model simulations that consider a combination of forcings. Recently, we applied a climate model to reproduce the YD climate in an experiment that was constrained through data-assimilation by proxy-based temperature reconstructions, primarily from the North Atlantic region (Renssen et al., 2015). The simulated temperatures were generally consistent with the proxy-based reconstructions for the YD climate, showing a marked cooling of 2–4 °C over the North Atlantic and the European continent. In addition, both the start and termination of the temperature anomaly were abrupt, in agreement with proxy data. Our simulation resulted in a global mean cooling of 0.6 °C that corresponds to independent estimates (Shakun and Carlson, 2010). This YD simulation was forced by a 3-year freshwater pulse of 5 Sv at the MacKenzie river outlet, a continuous meltwater forcing 0.1 Sv representing the background melt of the Fennoscandian and Laurentide icesheets, and a negative radiative forcing of −0.52 Wm^{-2}, representing the reduction in atmospheric methane and nitrous oxide, and enhanced mineral dust loading. In addition, the data assimilation procedure forced the model towards a state with anomalous atmospheric circulation over the North Atlantic region, promoting northerly atmospheric flow over Northwestern Europe (Renssen et al., 2015).

Here we extend our analysis of the same model experiment and present the global hydroclimatic response. We focus on the following questions:

- What is the global hydroclimatic response in our experiment constrained by temperature proxies, and how does it compare in magnitude and timing to the temperature response?
- To what extent is this hydroclimatic response consistent with proxy-based paleohydrological evidence?
- What mechanisms determine the global hydroclimatic response during the YD?

2. Methods

2.1. Model

We performed our simulations with the earth system model of intermediate complexity LOVECLIM, which consists of different components describing the oceans, sea ice, land surface, atmosphere, vegetation, land ice and carbon cycle (Goosse et al., 2010). In this study, we only activated the components for the ocean-atmosphere-sea ice-land surface-vegetation system. Hence, we prescribed the extent and elevation of all ice sheets, and also the meltwater fluxes associated with the melt of these ice sheets.

Since LOVECLIM is described in detail elsewhere (Goosse et al., 2010), we only provide a summary here. The atmospheric component is ECBilt, a global quasi-geostrophic model with three layers and a T21 spectral resolution (Opsteegh et al., 1998). A full hydrological cycle is included, with soil moisture being represented by a bucket model in the land surface model. When the bucket is full, the excess water is routed to the ocean as river runoff. The bucket volume depends on the simulated vegetation cover, with the volume being higher when the tree cover increases. ECBilt and the land surface model are coupled at the same grid resolution with VECODE, a simple dynamical vegetation model that describes the dynamics of two vegetation types – grassland and forest – and desert as a dummy type (Brovkin et al., 2002). The ocean-sea ice component is CLIO, consisting of an oceanic general circulation model with a 3° × 3° latitude-longitude resolution and 20 vertical layers, coupled to a dynamic-thermodynamic sea-ice model (Goosse and Fichefet, 1999). The ocean model includes parameterizations for eddy-induced tracer advection (Gent and McWilliams, 1990) and vertical mixing (Mellor and Yamada, 1982).

The version of LOVECLIM we use simulates a present-day climate that agrees reasonably well with modern observations (Goosse et al., 2010). LOVECLIM has a climate sensitivity to a doubling of CO_2 of 2.0 °C, which is in the lower range of other coupled climate models (Flato et al., 2013). In addition, the sensitivity of the ocean circulation to a freshwater perturbation is similar to that of AOGCMs (Stouffer et al., 2006; Renssen et al., 2015). LOVECLIM has been successfully used for many paleoclimate studies covering a range of periods, including previous interglacials (Yin and Berger, 2012; Bakker et al., 2014), the last glacial (Timmermann et al., 2004; Roche et al., 2007; Van Meerbeeck et al., 2009), the Younger Dryas (Renssen et al., 2015), the Holocene (Renssen et al., 2005, 2009; Blaschek and Renssen, 2013) and the last millennium (Goosse et al., 2005). In these studies, the response of LOVECLIM was found to be similar to that of more comprehensive models (Nikolova et al., 2013; Bakker et al., 2014; Renssen et al., 2015).

2.2. Experimental design

As a first step, we performed a 5000-year long spin-up experiment with forcings for 13 ka, representing the end of the relatively warm Allerød period (i.e. just before the start of the YD). The applied forcings include astronomical parameters (Berger, 1978), trace gas levels (Monnin et al., 2001; Spahni et al., 2005), and ice sheets (Suppl. Fig. 1, Peltier, 2004). It should be noted that we have not yet included the new updated parameterizations of the radiative forcing of CO_2, CH_4 and N_2O that were recently published (Etminan et al., 2016), probably leading to an underestimation of the methane radiative forcing. In this experiment and the ones that followed, we applied the land-sea distribution of the last glacial maximum. As a next step, we introduced background meltwater fluxes from the Laurentide and Fennoscandian ice sheets, both fixed at 0.05 Sv during 500 years. Compared to our spin-up, this caused a moderate cooling of the climate in the North Atlantic region due to a weakening of the AMOC's maximum strength from 20 to 16 Sv ($1\ Sv = 10^6\ m^3 s^{-1}$). The mean over the last century of these 500 years was selected to represent our **13 ka reference climate state**. As a final step, we perturbed this reference state to obtain the climate of the YD. As discussed in detail in Renssen et al. (2015), we performed a range of simulations in this third step, with various scenarios to evaluate the impact of different freshwater discharges and negative radiative forcing. We also applied a data-assimilation method (Dubinkina et al., 2011) to constrain the model in some of the experiments by proxy-based temperatures, taking into account their uncertainties. This so-called particle filter methodology used proxy-based 13ka minus 12 ka temperature anomaly estimates to select from a relatively large ensemble (i.e. a set of parallel simulations) those ensemble members that provided an optimal fit with the proxy-based estimates of the temperature change from the Allerød interstadial to the Younger Dryas. The proxy dataset is described in detail in Renssen et al. (2015), and consists primarily of chironomid-based July temperatures in Europe (Heiri et al., 2014), supplemented with a few annual SST estimates for the Nordic Seas, the Mediterranean Sea and the North Atlantic and North Pacific Oceans, and the annual mean temperature estimate based on Greenland ice cores. The same data-assimilation method has been applied extensively in several studies (Dubinkina et al., 2011; Mairesse et al., 2013; Mathiot et al., 2013).

Based on our evaluation, one particular experiment (**COMBINED**) driven by a combination of forcings and including data-assimilation, clearly provided the most consistent climate in comparison to proxy-based YD reconstructions (Renssen et al., 2015). This COMBINED experiment includes 96 ensemble members and lasted 1000 years with data assimilation turned on. The forcings consisted of the same background meltwater forcing as in our 13 ka reference run, plus an initial 3-year freshwater discharge of 5 Sv introduced at the start of the 1000 years at the MacKenzie River outlet, representing the drainage of Lake Agassiz. This was combined with a negative radiative forcing ($-0.52\ Wm^{-2}$ at the top of the troposphere), representing the effects of reduced atmospheric methane and nitrous oxide levels (Spahni et al., 2005; Schilt et al., 2010) and elevated atmospheric dust content (Mayewski et al., 1993; Alley, 2000). As a response to these forcings, the AMOC weakened to 7 Sv and the climate cooled substantially, especially in the North Atlantic region.

After these 1000 years of simulation in COMBINED, we continued the experiments in two different ways to investigate the recovery from the perturbed state. In one scenario (**NO_BGMF**), we removed the background melt flux, but kept the negative radiative forcing and the data assimilation towards the proxy-based YD temperature anomalies. The removal of the background melt flux caused a reinvigoration of the AMOC and a rapid warming in the Northern Hemisphere, reminiscent to the end of YD as registered in proxy records. We sustained this scenario for another 500 years. In a second contrasting scenario (**NO_DAR**), we continued the background melt flux, but we switched off the data assimilation and removed the negative radiative forcing. By comparing the difference in the climate response to these two scenarios, we are able to differentiate between the impact of the AMOC weakening on the one hand (NO_BGMF) and the combined effect of the negative radiative forcing and data assimilation on the other hand (NO_DAR). We performed no recovery experiment with all forcings (i.e. background melt flux, radiative forcing) turned off and no data assimilation.

In this paper, we will analyze the global, annual mean hydroclimatic response in the COMBINED experiment and the two recovery scenarios. The results displayed are the weighted averages of the 96-member ensemble, with weights function of the likelihood of each member (Dubinkina et al., 2011). To estimate the duration of the initial and recovery phases of the simulated anomalies, we fitted a ramp function through the raw simulated data following Mudelsee (2000).

3. Results

3.1. General temperature response

We find the strongest temperature response in the North Atlantic region, where LOVECLIM simulates an annual mean cooling of more than 4 °C over the Nordic Seas, the Labrador Sea and coastal regions of northern Scandinavia (Fig. 1a). Over much of Eurasia and North Africa, the cooling is larger than 1 °C. In North America, the cooling is generally less expressed, with values mostly between −0.5 and −1 °C. In the tropics, a small cooling of less than 0.5 °C is simulated over most continents. Over continents south of 30°S, such as Australia, the temperature response is less than the ±2 standard deviation level of our 500-year long simulation with fixed 13 ka forcings (see Section 2.2).

Over the SH oceans, there are a few regions with a slight, but significant warming, most notably in the Indian Ocean sector of the Southern Ocean where temperatures are more than 0.5 °C above the 13 ka reference level. In the Atlantic Sector, there are relatively large areas with cooling around 60°S, but also patches with small warming.

3.2. General hydroclimate response

To analyze the hydroclimate response, we focus on the simulated change in soil moisture, as it provides an indication of the overall moisture availability, taking into account the combined effect of precipitation, evaporation, snowmelt and surface runoff. We expect that the simulated soil moisture is the model variable that generally is closest to proxy-based evidence for changes in hydroclimate. In our results, the simulated changes in precipitation clearly dominate the soil moisture response in most regions. For reference, we provide the precipitation changes in the supplementary information (Supplementary Figs. 2–4). In Fig. 1b, the response in soil moisture that is outside one standard deviation of the 500-year long simulation with 13ka forcings is plotted, showing a complex spatial pattern, with some areas experiencing more moisture, while other areas are drier. Most of mid and high latitude Eurasia shows a marked decrease in soil moisture, with NE Europe as a notable exception. In Southeast Asia, a clear decrease is found north of the equator, neighboring a region with increase south of the equator down to Northern Australia. In Africa, a belt with clearly drier conditions stands out between 5 and 15°N that continues into Arabia. In contrast, at 20°S in SW Africa there is more

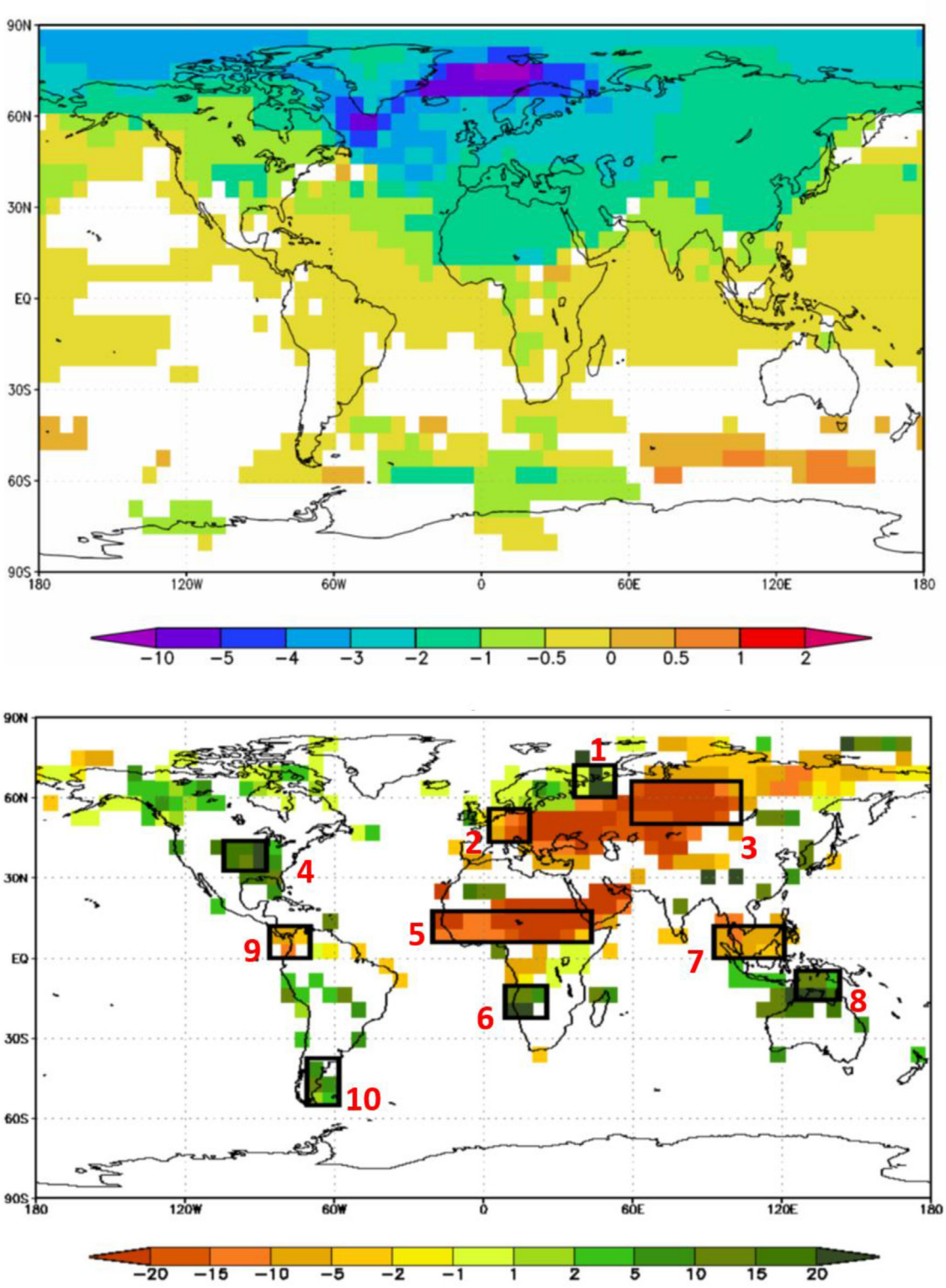

Fig. 1. a (top): Simulated mean annual temperature anomaly (°C) in the COMBINED experiment relative to the 13 ka reference climate. Results are only shown where they exceed the ±2-standard deviation level of our 500-year long simulation with fixed 13 ka forcings. Fig. 1b (bottom) Simulated mean annual change in soil moisture (in %) in the COMBINED experiment relative to the 13 ka reference climate. The original unit is in metres, but changes are shown as percentages to facilitate interpretation. Only results exceeding the ±1-standard deviation level of the 13 ka climate are shown. The thick-lined boxes indicate the regions that are analyzed in detail: 1) Northeastern Europe, 2) Central Europe, 3) Western Siberia, 4) southeast North America, 5) Sahel, 6) Southwest Africa, 7) Southeast Asia, 8) Northern Australia, 9) Central America, 10) southern South America.

humidity. In Southeast North America, there is an area with a marked increase in soil moisture. In addition, dryness prevails along the northern coast of South America, while at the southern tip of South America wetter conditions are simulated.

Based on this global response in soil moisture, we selected 10 regions from different continents for a detailed temporal analysis. Our goal was to select regions with a clear response in soil moisture (i.e. outside the 1σ level of the reference climate) and with a good global coverage (i.e. from different continents and climatic zones). We present the locations of these regions in the map with the mean annual soil moisture anomaly (Fig. 1b). The results for these regions are from areas covering at least six land-grid cells.

3.3. Regional response

For the 10 considered continental regions, we estimated the durations of the onset and recovery phases based on a fitted ramp function (Mudelsee, 2000), using only the NO_BGMF recovery scenario because this shows the clearest recovery. These durations are provided in Fig. 2a–b. In regions in the southern hemisphere, the recovery in temperature was not clear enough to fit a ramp function. In the following sections, we discuss the simulated evolutions in surface temperature and soil moisture. Except for Northeastern Europe, the changes in soil moisture are primarily determined by the changes in precipitation, as shown by the very similar responses and the high temporal correlation between annual mean time series of these two variables (>0.94). In Northeastern Europe, the soil moisture is also determined by changes in evaporation. For reference, we provide the simulated time-series of precipitation for the 10 regions in the supplementary information.

3.3.1. YD initial phase

All considered continental regions experience a clear cooling (Fig. 3). The magnitude of this YD cooling is strongest over continents under direct influence of the cold North Atlantic Ocean and decreases steadily in regions further away, such as the Southern Hemisphere tropics (Fig. 4). Although the simulated cooling outside the North Atlantic region is relatively small (less than 1 °C), the temperature decrease is in all cases abrupt (within 100 years, Fig. 2a) and clearly outside the 2-sigma level of the 13k reference climate. In central and NE Europe and the Sahel region, the initial cooling can be divided in a rapid first phase within 15 years and a more gradual second phase.

Compared to the temperature response, the initial response in soil moisture is much more diverse among the considered regions, showing both marked increases and decreases, of varying duration (Figs. 2a and 3). The response in the tropics shows a coherent pattern, with a clear reduction over continents in the Northern Hemisphere, and a marked rise in soil moisture in the Southern Hemisphere continents. In the tropics, the start of the soil moisture anomalies is relatively gradual and takes more than twice as long as the more sudden decline in temperature (Fig. 2a). Here, typically the initial response in soil moisture lasts 100 years or more, whereas the cooling takes only a few decades at most. This gradual response is also seen in the simulated precipitation (Suppl. Fig. 4). In the Northern Hemisphere extratropics, on the other hand, the soil moisture response has a more similar duration as the cooling. Over most of mid- and high latitude Eurasia there is a distinct decrease in soil moisture (Fig. 3b and f). Northeastern Europe forms a notable exception with a clear soil moisture increase that is much faster (within 20 years) than the response in temperature (more than 70 years, Fig. 3d). Southeast North America is also becoming wetter (Fig. 3h).

3.3.2. YD recovery phase

On continents directly affected by the North Atlantic Ocean, the temperature displays a clear recovery in the NO_BGMF scenario, revealing the dominant impact of the AMOC weakening on the cooling (Fig. 3a,c,e, i). The NO_DAR scenario only causes a notable 0.6 °C warming in NE Europe, suggesting that a substantial part of the overall simulated YD cooling here can be attributed to the associated increase in northerly winds driven by the data assimilation (Renssen et al., 2015) and the negative radiative forcing. In contrast, the NO_DAR scenario dominated the temperature recovery in some regions in the Southern Hemisphere, particularly North Australia and Southern South America (Fig. 3o, s). In the remaining regions, both scenarios display a clear recovery, for example in SE North America and SW Africa (Fig. 3g, q). In the Northern Hemisphere, the temperature recovery lasts about 100 years and takes substantially longer than the initial cooling phase in the North Atlantic region (Fig. 2a and b).

The soil moisture recovery is in all cases much larger in the NO_BGMF scenario (Fig. 3), showing the importance of the Atlantic Ocean circulation for the hydroclimate. In the tropics, this provides a clear contrast to the temperature recovery that was larger in the NO_DAR scenario. The duration of the soil moisture recovery is about 130 years in the tropics and Western Siberia and notably shorter in the remaining regions (Fig. 2b). Especially in Northeastern Europe and Southeastern North America, the recovery is rapid (less than 50 years). The NO_DAR scenario has a clear impact on the soil moisture recovery in SE North America (Fig. 3h).

3.4. Comparison with proxy data: hydroclimate

Our simulated global YD hydroclimate anomaly is generally in agreement with the signal that is revealed by various proxy data (compare Fig. 1b with Fig. 5). The contrast in simulated hydroclimate response between Southeast Asia and Northern Australia is in agreement with evidence from speleothems. Griffiths et al. (2010) reconstructed an increase in monsoon rainfall during the YD in Southern Indonesia (within our box for Northern Australia), whereas Partin et al. (2015) inferred drier conditions in a speleothem record from the Philippines (in our Southeast Asia box). This contrasting cross-equatorial pattern is supported by numerous data as reviewed by Partin et al. (2015). Moreover, the latter study also concluded that the hydroclimate response in the tropics was much more gradual than the temperature response in the North Atlantic, which also agrees with our results. Besides, our model does not capture the full effect of a weakened Asian monsoon and drier conditions as was reconstructed based on speleothems in southern China (Wang et al., 2001) and suggested by lake level changes and pollen-based precipitation reconstructions in northern China (Chen et al., 2015; Goldsmith et al., 2017). In our simulations, the reduced humidity is restricted to Southeast Asia, extending to northern India (Fig. 1b).

The marked drying of tropical Africa in our results is consistent with several reconstructions based on lake levels and leaf-wax biomarker data (Fig. 5), indicating a significantly drier climate here during the YD (Gasse, 2000; Shanahan et al., 2015). Likewise, pollen-based evidence from Southwest Africa support a wetter climate here (Fig. 5) in agreement with our model results (Shi et al., 2000; DuPont et al., 2004). However, our simulation has not captured the dry conditions that have been inferred from lake studies in Eastern Africa (Fig. 5, Lake Malawi and Lake Tanganyika, Talbot et al., 2007), but this may be related to the strong biases of LOVECLIM in this region (Goosse et al., 2010).

The reduction in soil moisture simulated for Central America fits with data from Cariaco Basin indicating dry conditions during YD time (Haug et al., 2001). The relatively dry conditions

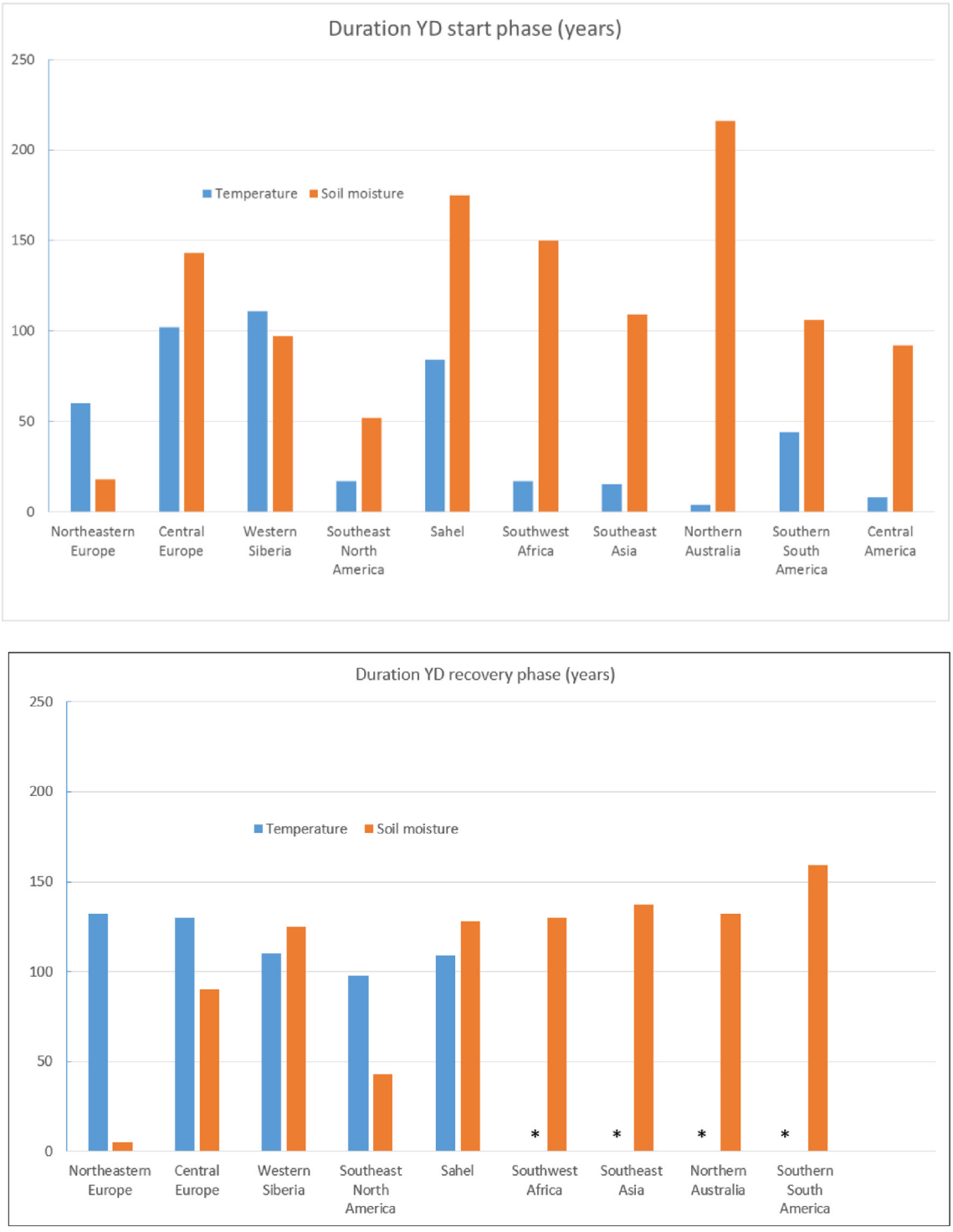

Fig. 2. Duration (in years) of the onset and recovery phases in the regions indicated in Fig. 1b. The duration is based on a ramp function (Mudelsee, 2000) fitted through the annual simulation results. Fig. 2a (top), onset phase and Fig. 2b (bottom), recovery phase. The stars (*) indicate that fitting a ramp function was not possible for the temperature time-series, due too small changes during the recovery phase. This is also the case for both temperature and soil moisture in Central America (see Fig. 3m,n).

reconstructed based on Andean glacier data south of the equator (Colombia, Jomelli et al., 2014) is not seen in our simulations. However, lake level evidence from the same region (Bolivia) suggests that the climate was relatively wet during the YD (Baker et al., 2001), which would support our simulation results that show an increase in soil moisture. The relatively wet conditions simulated in southern and central North America agrees with numerous lines of evidence (Fig. 5), including pollen and plant-macrofossil data from Florida, speleothems from Arizona (Wagner et al., 2010) and New Mexico (Polyak et al., 2004) and isotopic data from cellulose and leaf water from mid-continental sites (Voelker et al., 2015). Proxy data from southern South America clearly indicate wet and cold conditions during the Antarctic Cold Reversal (14.7–13.0 ka), as reflected by evidence

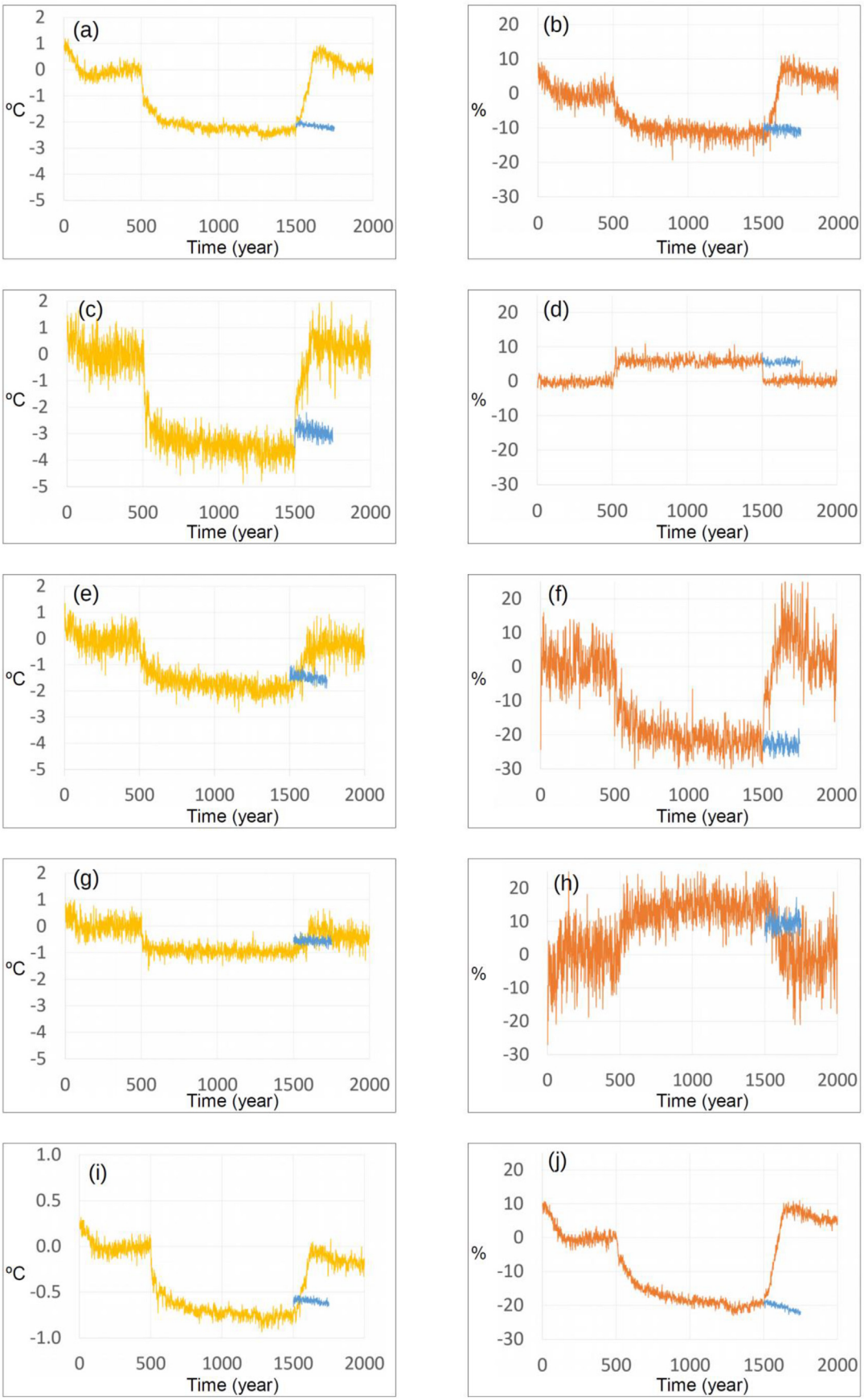

Fig. 3. a-t (next 2 pages). Simulated annual changes in surface temperature (yellow, in °C) and soil moisture (orange, in %). The reference climate is represented by year 401–500. The COMBINED experiment covers years 501–1500, with a 5Sv freshwater pulse being added in years 501–503 to the Arctic Ocean at the MacKenzie River outlet. The yellow or orange results for years 1501–2000 represent the NO_BGMF scenario, while the results of the NO_DAR scenario are provided in blue. (a,b) Central Europe, (c,d) Northeast Europe, (e,f) Western Siberia, (g,h) Southeastern North America, (i,j) Sahel region, (k,l) Southeast Asia, (m,n) Central America, (o,p) Southern South America, (q,r) Southwest Africa, (s,t) Northern Australia. (For interpretation of the references to colour in this figure legend, the reader is referred to the Web version of this article.)

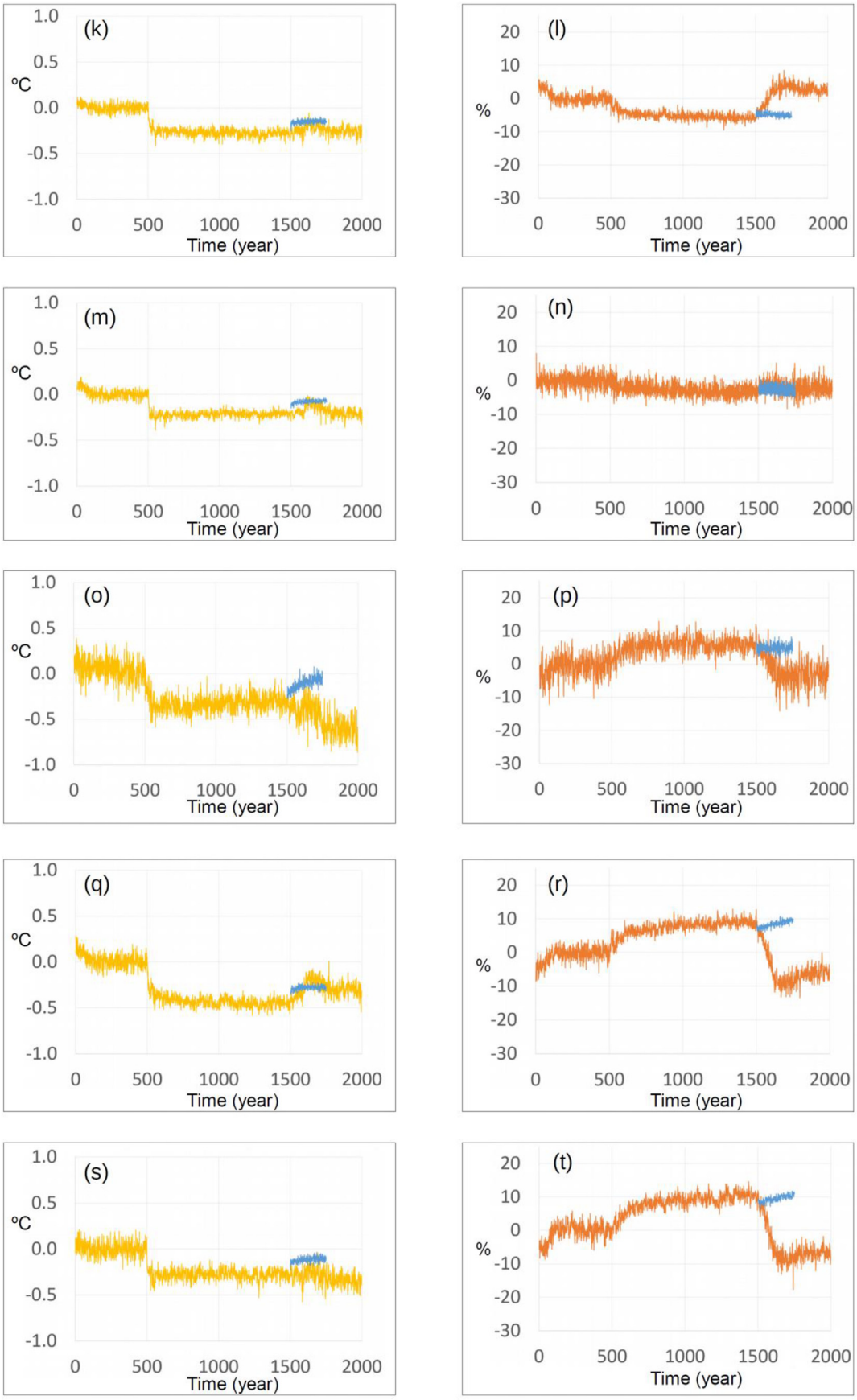

Fig. 3. (*continued*).

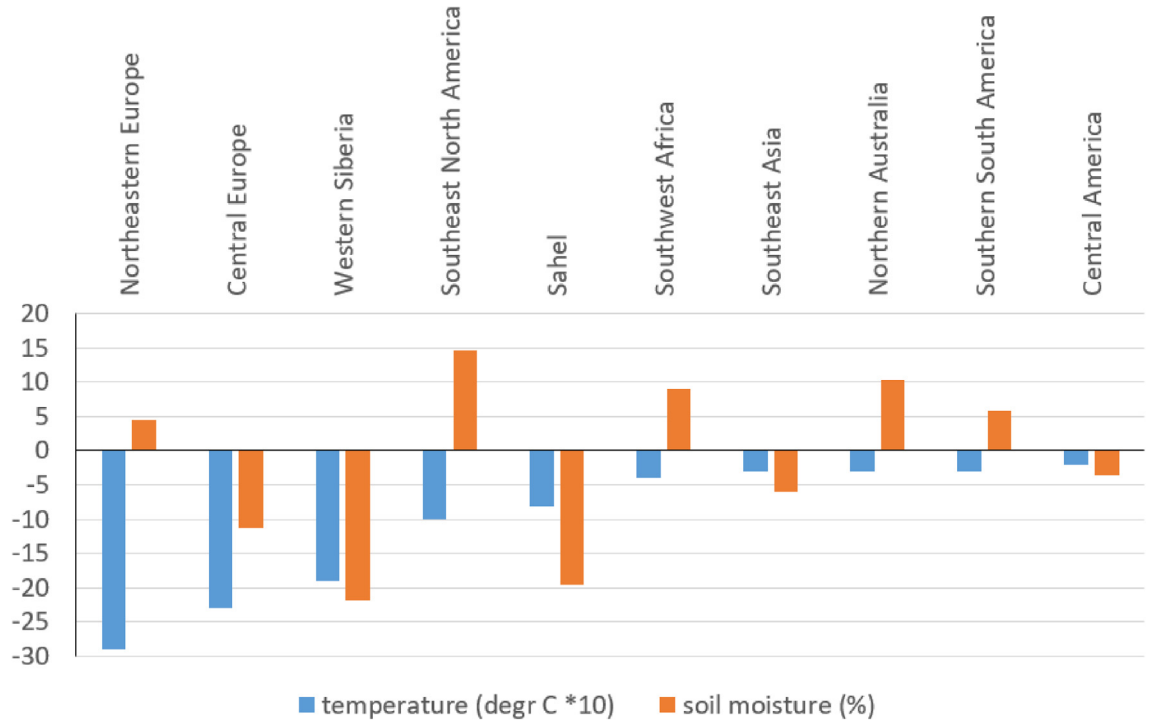

Fig. 4. Mean response in temperature and soil moisture for the ten considered regions. Shown are the differences between years 1401–1500 and 401–500 (13ka reference climate).

for glacier readvances and pollen records (e.g., Moreno and Videla, 2016; Graham et al., 2016). These cold and wet conditions appear to extend into the YD (Moreno et al., 2009; Moreno and Videla, 2016), compatible with our simulation results.

Our results for Central Europe are consistent with speleothem data from France (Genty et al., 2006), suggesting an abrupt decrease in humidity at onset of the YD. These speleothem data even suggest a higher rate of change (about 80 years for the onset) than our simulations. A detailed study based on sedimentary lipid D/H ratios from a lake in Germany confirms these dry conditions (Rach et al. (2017). A comparison of our simulated soil moisture anomaly with their reconstruction of relative humidity shows a very similar magnitude of drying, and rates of change, including an overshoot after the transition to the Holocene that is similar to our simulated result (Fig. 6). However, the data from Germany also suggest that the reduced moisture availability is delayed compared to the local cooling (Rach et al., 2014). We do not simulate a lag in the hydroclimate response here, but find that the decrease in moisture is more gradual than the cooling. Furthermore, our simulated YD anomaly lasts ~100 year longer than the reconstructed humidity signal, which is related to the timing of the removal of the

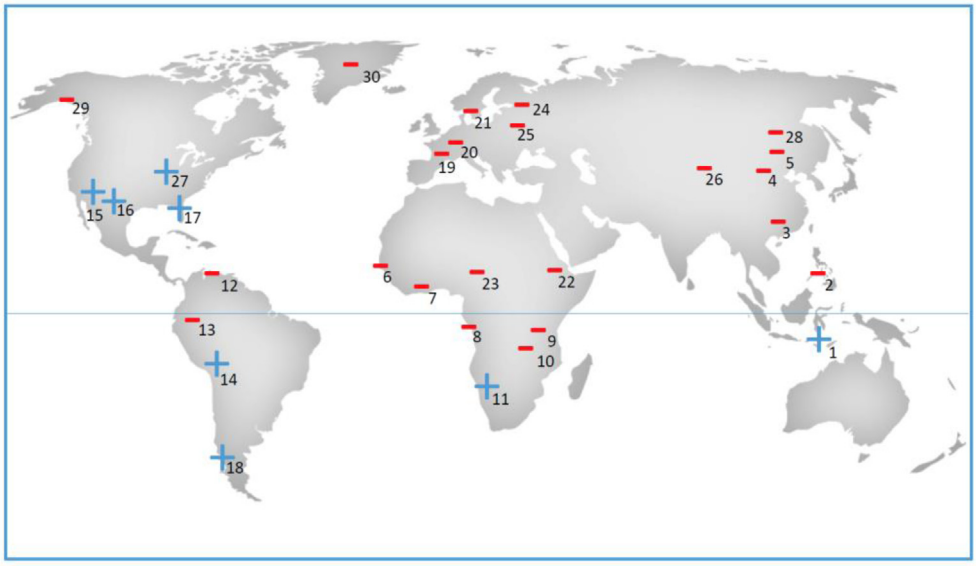

Fig. 5. Global proxy-based hydroclimatic signal during the YD, based on selected proxy data. A minus ('-') indicates a reduction in humidity, while a plus ('+') detects a wetter climate during the YD. The numbers refer to Supplementary Table 1.

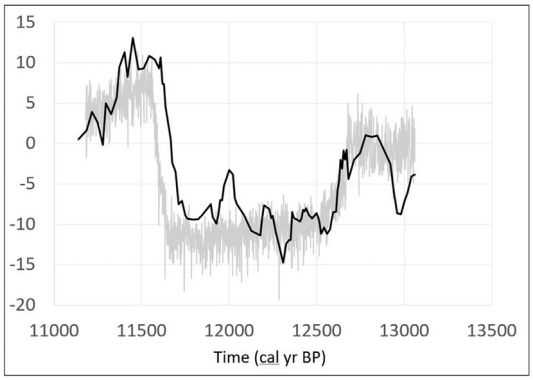

Fig. 6. Comparison of the simulated soil moisture signal for Central Europe (cf. Fig. 3b, NO_BGMF) with the relative humidity reconstruction of Rach et al. (2017) based on sedimentary lipid D/H ratios from Lake Meerfelder Maar in Germany. Both datasets are plotted as percentage change from the climate before the YD anomaly. Time is given in cal yr BP and is running from right to left as in Rach et al. (2017), in contrast to Fig. 3. We have plotted their Δrh** solution. For the timescale of the model result it is assumed that the YD start (12680 cal BP) equals model year 501 (i.e. when COMBINED starts in Fig. 3).

background meltwater forcing in our experiments. The drier conditions in Europe are also recorded further north in Southern Sweden (Muschitiello et al., 2015). We have found no indication in proxy-based reconstructions for the wetter conditions in northeastern Europe suggested by our model experiments, since proxy records from northwest Russia indicate drier conditions (Subetto et al., 2002; Wohlfarth et al., 2002; Novenko et al., 2009).

To evaluate our model result over Greenland, we compare the simulated accumulation with equivalent ice core data (Alley, 2000) from GISP2 (Suppl. Fig. 5). Our model captures the main declining trend at the YD start, but suggests a larger reduction during the event. At the end of the YD, the magnitude of the initial recovery is similar in both cases, but the applied NO_BGMF scenario does not lead to full recovery as in the GISP2 data.

4. Discussion

4.1. Impact of different forcings

The AMOC weakening is the dominant cause for the changes in soil moisture in all regions considered, including those in the Southern Hemisphere (Fig. 7). At low latitudes, the simulated changes in soil moisture are related to a southward shift in the ITCZ, as has also been described in other model studies in which the Atlantic Ocean circulation was weakened by freshwater perturbations (e.g., Stouffer et al., 2006; He et al., 2013; Mohtadi et al., 2014). The cooling of the Northern Hemisphere, especially the North Atlantic, results in a dipole pattern in the simulated precipitation anomaly, with negative anomalies over the relatively cold northern tropics, and positive anomalies south of the equator (Suppl. Fig 2).

In our model result, this cross-equatorial contrast is especially clear over the Indian Ocean (Suppl. Fig. 2) and is also evident in the zonal average precipitation anomaly (Suppl. Fig. 3). These precipitation anomalies are associated with a reorganization of the mean Hadley Cell circulation, with a southward shift of the upward branch (i.e. ITCZ) and enhanced upper-level cross-equatorial flow. In other modelling studies with more comprehensive models, these changes have been described in detail (e.g., Stouffer et al., 2006; Frierson et al., 2013; Mohtadi et al., 2014). There is an important seasonal aspect in this response, as in COMBINED the changes in precipitation are primarily associated with the local rainy season: the decrease in precipitation north of the equator has a maximum in June to September, whereas the increase in the Southern tropics peaks in October to April. The simulated temporal moisture response at low latitudes is relatively gradual (more than 100 years), indicating that the impact of the ITCZ shift steadily builds up. This is also reflected in the difference between the time-evolution of the long-distance meridional gradient (between the North Atlantic and the southern tropical oceans) that drives the ITCZ shift, and the local temperature response in the tropics (Suppl. Fig. 6). The local cooling is at least 100 years faster than the full build-up of the meridional temperature contrast.

The dry conditions in Central Europe and Western Siberia are

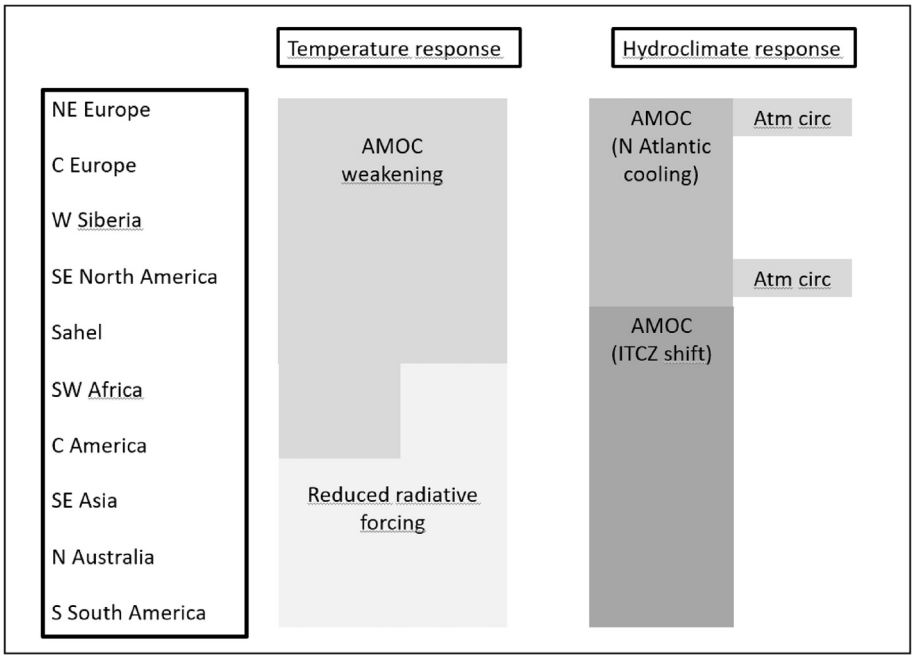

Fig. 7. Overview of the dominant drivers of the response in temperature and hydroclimate in our YD simulation.

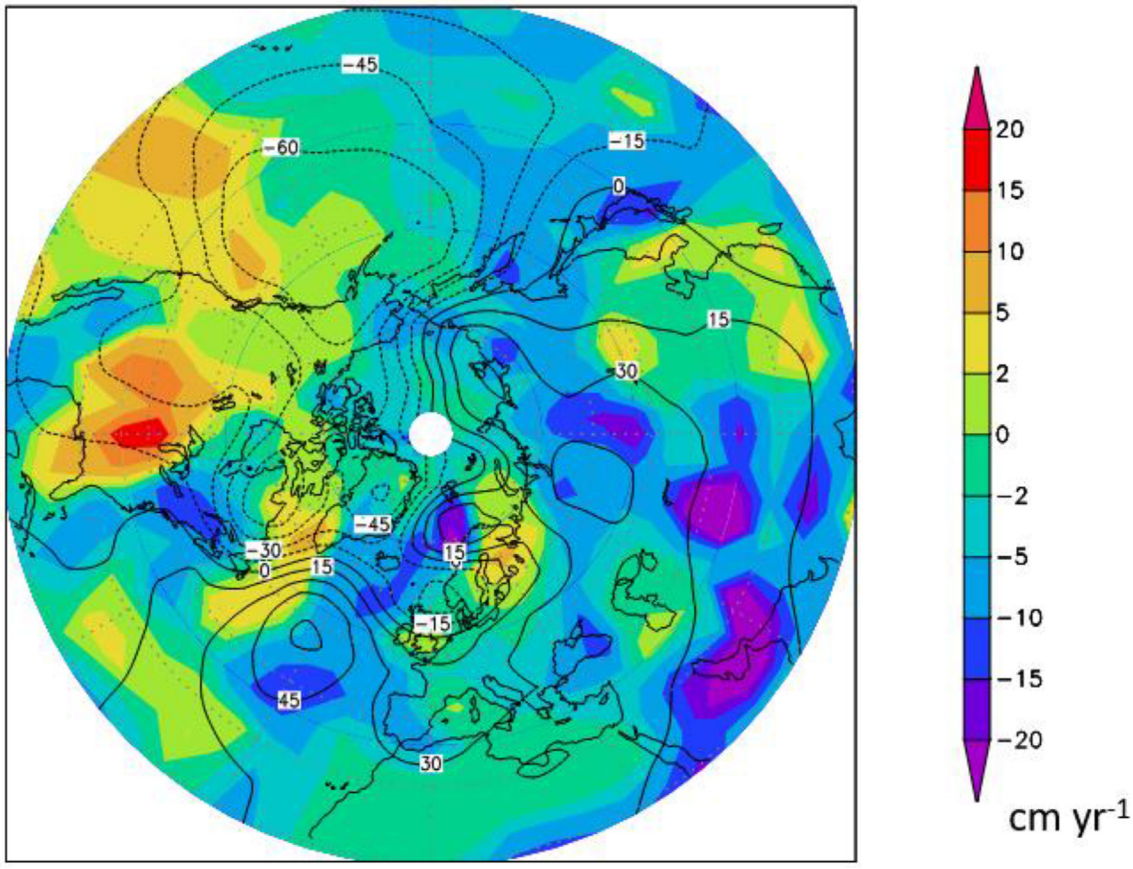

Fig. 8. Simulated AMJJA (April-to-August) anomaly in precipitation (shaded) and 800 hPa geopotential height (contours, in m^2s^{-2}) between COMBINED and the unperturbed 13 ka reference climate.

related to the strong cooling due to the AMOC weakening, reducing the moisture content of the air masses transported inland by westerlies. The good match of our simulated soil moisture anomaly with the detailed relative humidity reconstruction in Germany of Rach et al. (2017) suggests that our simulation with COMBINED and NO_BGMF captures well the mechanism for drying in Europe (Fig. 6). The overshoot after the recovery that is visible in both model and data is directly linked to a similar overshoot in the AMOC strength and North Atlantic sea surface temperatures (Renssen et al., 2015, their Fig. 3c).

In two areas, other forcings besides the AMOC weakening are also important for the soil moisture response. These two areas are Northeastern Europe and Southeastern North America, where the soil moisture increased relatively rapidly in our COMBINED experiment. A seasonal analysis of these relatively wet soil conditions in Northeastern Europe (Fig. 3c and d) and Southeastern North America (Fig. 3g and h) shows that these originate in the summer season. In our earlier study (Renssen et al., 2015), we showed that in COMBINED a change in atmospheric circulation was simulated in summer, with relatively high pressure over the cold North Atlantic Ocean and reduced surface pressure over the North Sea, resulting in anomalous northerly flow, bringing cold polar air southwards over Northwestern Europe (Fig. 8). However, more to the east, at the eastern flank of this negative pressure anomaly, an anomalous southerly flow was generated, transporting relatively moist air towards Northeastern Europe, explaining the increase in moisture in this region. Sensitivity experiments with only one forcing performed by Renssen et al. (2015) revealed that the data assimilation, the reduced radiative forcing and the AMOC weakening all contributed to this change in atmospheric circulation. However, the resulting wetter conditions in northeastern Europe do not match with climate reconstructions that suggest a drier climate in the same region. Yet, proxy-based hydroclimatic reconstructions are scarce in this area, and possibly, our low-resolution model has not captured the right location of the wet anomaly. Further research should therefore reveal if there really was a region with a wetter climate in northeastern Europe. The change in atmospheric circulation also affected North America, as in our COMBINED experiment a positive pressure anomaly was present over eastern North America, and a negative anomaly over western North America (Fig. 8). The result was a southerly flow bringing moist air from the Gulf of Mexico northwards to the American continental interior, resulting in enhanced soil moisture levels there, in agreement with proxy evidence (e.g., Polyak et al., 2004; Grimm et al., 2006).

Regarding the temperature response, the reduction in AMOC strength is only dominating the cooling in areas under direct influence of the North Atlantic Ocean. These areas include Northeastern and Central Europe, Western Siberia, Southeastern North America and the Sahel region. In most regions considered in the Southern Hemisphere, the reduction in radiative forcing is mainly responsible for the temperature decrease. In these areas, the cooling is relatively modest (−0.2 to −0.4 °C). In the areas affected directly by the Atlantic Ocean, the NO_DAR recovery scenario shows that the radiative forcing actually leads to a cooling of a similar magnitude as in the Southern Hemisphere, but here this effect is overwhelmed by the impact of the AMOC weakening. In some areas, notably Southwest Africa and Central America, the

AMOC weakening and the negative radiative forcing have a similar contribution to the overall cooling in COMBINED.

In our experiments, we reduced the radiative forcing instantaneously everywhere at the start of COMBINED. In reality, the decline in radiative forcing would have taken more time, as it also depends on the climate change itself. In particular, estimates from ice cores suggest that the 230 ppb decrease in atmospheric methane levels took 340 years (Brook and Severinghaus, 2011). However, the rise in atmospheric dust levels was probably much faster (within two decades, e.g., Alley, 2000; Steffensen et al., 2008), but it is expected that there were large spatial variations in the associated radiative forcing. In particular, dust records from Greenland, Antarctica and the Tropical North Atlantic Ocean suggest that the amount of dust in the atmosphere strongly depends on the latitude (DeMenocal et al., 2000; Steffensen et al., 2008; Schüpbach et al., 2013). Overall, this implies that our COMBINED experiment certainly overestimates the rate of cooling in areas where the temperature decrease is governed by the radiative forcing. This is relevant for the considered areas in the Southern Hemisphere where the onset phase of the simulated cooling lasted about 20 years (Fig. 2a).

In addition, other modelling studies addressing the Younger Dryas show warming at some Southern Hemisphere continents. This is for instance the case in the experiments of He et al. (2013), showing relatively high temperatures over parts of South America and Southern Africa. These warmer conditions are associated with the so-called bi-polar seesaw effect, with AMOC weakening leading to cooling in the North Atlantic, but accumulation of heat and warming in the South Atlantic and the Southern Ocean. Our model is known to generate a relatively modest bi-polar seesaw effect compared to other global models (Stouffer et al., 2006) and with quite a long delay in the Southern Ocean (of about one century, c.f., Roche et al., 2010). This bi-polar seesaw effect is weakly present in our results, generating a warmer Southern Ocean in the Indian Ocean sector (Fig. 1a). However, in our simulation this Southern Hemisphere warming is modest, and is not strong enough to overwhelm the continental cooling produced by the reduction of radiative forcing. In simulations that consider both freshwater and negative radiative forcing, the sign of the temperature anomaly (i.e. cooling or warming) in the Southern Hemisphere thus depends on the magnitude of the AMOC weakening. Potentially, proxy-based temperature reconstructions could provide evidence of either warming or cooling on Southern Hemisphere continents. Available temperature reconstructions from the Southern Hemisphere generally suggest small warming of less than 1 °C, although some sites also record cooling (Shakun and Carlson, 2010). However, these reconstructions are mostly based on marine sediment cores, and thus provide limited information on the climate conditions on the continents. Our simulations suggest that a YD cooling in the Southern Hemisphere would be less than 0.5 °C, which is probably within the uncertainty of most proxies. In any case, our simulated value of 0.6 °C global mean cooling during the YD event matches the independent estimate of Shakun and Carlson (2010). Since our estimate for cooling in the Northern Hemisphere matches well with proxy evidence, this supports our simulation as a reasonable representation of the global YD climate.

4.2. Temperature vs hydroclimate response

In the areas under direct influence of the Atlantic Ocean, the responses in temperature and soil moisture are in line and show similar rates of change and timing. In contrast, in the other regions, the temperature and soil moisture are decoupled, indicating very different responses. These areas are all located in the tropics and/or Southern Hemisphere, where the cooling is a response to the negative radiative forcing, while the hydroclimatic changes are mainly resulting from the shifts in the ITCZ. This has important consequences for the interpretation of hydroclimatic proxy records from these regions, as it implies that such data should not be directly related to key records from high latitudes, such as ice core stable isotope records.

5. Conclusions

We analyzed the global response in temperature and soil moisture in transient simulations of the Younger Dryas climate. Our results generally agree with proxy-based evidence and suggest the following:

- Both the temperature and hydroclimate responses clearly have a global signature. The cooling is most expressed over the North Atlantic Ocean (more than 5 °C) and downwind continents (2–4 °C), which is related to the weakening of the AMOC under influence of meltwater discharge. The hydroclimate response is strongest over Eurasia in a belt between 40 and 60°N and North Africa in the Sahel region. In both areas, a strong decrease in soil moisture is simulated (of about −20%). The strongest increase in moisture is found in southeastern North America (+15%), where southerly atmospheric flow brings moist air inland.
- Outside the regions directly influenced by the strong cooling of the North Atlantic Ocean, the responses of temperature and moisture are decoupled. In other words, the causes of the temperature and hydroclimate responses are not the same at these locations.
- In the tropics, the hydroclimate response is governed by the southward shift of the ITCZ due to cooling of the North Atlantic Ocean. This causes drier conditions north of the equator, in particular in Northern Africa, Central America and Southeast Asia, and wetter conditions in the Southern Hemisphere tropics, such as in Southern Indonesia, Northern Australia, Southwest Africa and the southern part of South America. The associated changes in soil moisture are relatively gradual (taking up to two centuries), suggesting that the impact of the ITCZ shift on the tropical hydroclimate is building up.
- Our simulations suggest that continents in the Southern Hemisphere experienced a small cooling (less than 0.5 °C) during the YD, to mimic the negative radiative forcing associated with lowered methane concentrations and elevated atmospheric dust levels. In our experiment, the bipolar seesaw mechanism is not very strong, so that the associated warming influence of the South Atlantic Ocean is not overwhelming the radiative cooling.

Acknowledgements

H.R. was supported by visiting researcher grants of the Université catholique de Louvain and Institut Pierre Simon Laplace. Hugues Goosse is research director with the FRS/FNRS, Belgium. D.M.R. is supported by CNRS and VU-Amsterdam.

Appendix A. Supplementary data

Supplementary data related to this article can be found at https://doi.org/10.1016/j.quascirev.2018.05.033.

References

Alley, R.B., 2000. The Younger Dryas cold interval as viewed from central Greenland. Quat. Sci. Rev. 19, 213–226.
Baker, P.A., et al., 2001. Tropical climate changes at millennial and orbital timescales

on the Bolivian Altiplano. Nature 409, 698–701.
Bakker, P., Masson-Delmotte, V., Martrat, B., Charbit, S., Renssen, H., Gröger, M., Krebs-Kanzow, U., Lohman, G., Lunt, D.J., Pfeiffer, M., Phipps, S.J., Prange, M., Ritz, S.P., Schulz, M., Stenni, B., Stone, E.J., Varma, V., 2014. Temperature trends during the Present and Last interglacial periods: a multi-model-data comparison. Quat. Sci. Rev. 99, 224–243. https://doi.org/10.1016/j.quascirev.2014.06.031.
Berger, A.L., 1978. Long-term variations of caloric insolation resulting from earths orbital elements. Quat. Res. 9, 139–167.
Blaschek, M., Renssen, H., 2013. The Holocene thermal maximum in the Nordic Seas: the impact of Greenland Ice Sheet melt and other forcings in a coupled atmosphere-sea ice-ocean model. Clim. Past 9, 1629–1643.
Brook, E.J., Severinghaus, J.P., 2011. Methane and megafauna. Nat. Geosci. 4, 1–2.
Brovkin, V., Bendtsen, J., Claussen, M., Ganopolski, A., Kubatzki, C., Petoukhov, V., Andreev, A., 2002. Carbon cycle, vegetation and climate dynamics in the Holocene: experiments with the CLIMBER-2 model. Global Biogeochem. Cycles 16, 1139. https://doi.org/10.1029/2001GB001662.
Carlson, A.E., 2013. The younger Dryas climate event. In: Elias, S.A. (Ed.), The Encyclopedia of Quaternary Science, vol 3. Elsevier, Amsterdam, pp. 126–134.
Chen, F., Xu, Q., Chen, J., Birks, H.J.B., Liu, J., Zhang, S., Jin, L., An, C., Telford, R.J., Cao, X., Wang, Z., Zhang, X., Selvaraj, K., Lu, H., Li, Y., Zheng, Z., Wang, H., Zhou, A., Dong, G., Zhang, J., Huang, X., Bloemendal, J., Rao, Z., 2015. East Asian summer monsoon precipitation variability since the last deglaciation. Sci. Rep. 5 https://doi.org/10.1038/srep11186.
DeMenocal, P., Ortiz, J., Guilderson, T., Sarnthein, M., 2000. Coherent high- and low latitude climate variability during the Holocene warm period. Science 288, 2198–2202.
Dorale, J.A., et al., 2010. Isotopic evidence for younger Dryas aridity in the north American midcontinent. Geology 38, 519–522. https://doi.org/10.1130/G30781.1.
Dubinkina, S., Goosse, H., Damas-Sallaz, Y., Crespin, E., Crucifix, M., 2011. Testing a particle filter to reconstruct climate changes over the past centuries. Int. J. Bifurcat. Chaos 21, 3611–3618.
Dupont, L., et al., 2004. Southwest African climate independent of Atlantic sea surface temperatures during the Younger Dryas. Quat. Res. 61, 318–324.
Etminan, M., et al., 2016. Radiative forcing of carbon dioxide, methane, and nitrous oxide: a significant revision of the methane radiative forcing. Geophys. Res. Lett. 43, 12614–12623. https://doi.org/10.1002/2016GL071930.
Flato, G., et al., 2013. Evaluation of climate models. In: climate change 2013: the physical science basis. In: Stocker, T.F., et al. (Eds.), Contribution of Working Group I to the 5th Assessment Report of the IPCC. Cambridge University Press, NY, USA, pp. 741–866. Cambridge, United Kingdom and New York.
Frierson, D.M.W., et al., 2013. Contribution of ocean overturning circulation to tropical rainfall peak in the Northern Hemisphere. Nat. Geosci. 6, 940–944.
Gasse, F., 2000. Hydrological changes in the African tropics since the last glacial maximum. Quat. Sci. Rev. 19, 189–211.
Gent, P.R., McWilliams, J.C., 1990. Isopycnal mixing in ocean general circulation models. J. Phys. Oceanogr. 20, 150–155.
Genty, D., et al., 2006. Timing and dynamics of the last deglaciation from European and North African d13C stalagmite profiles—comparison with Chinese and South Hemisphere stalagmites. Quat. Sci. Rev. 25, 2118–2142.
Goldsmith, Y., et al., 2017. Northward extent of East Asian monsoon covaries with intensity on orbital and millennial timescales. Proc. Natl. Acad. Sci. Unit. States Am. 114, 1817–1821.
Goosse, H., Fichefet, T., 1999. Importance of ice-ocean interactions for the global ocean circulation: a model study. J. Geophys. Res. 104, 23337–23355.
Goosse, H., Renssen, H., Timmermann, A., Bradley, R.S., 2005. Internal and forced climate variability during the last millennium: a model-data comparison using ensemble simulations. Quat. Sci. Rev. 24, 1345–1360.
Goosse, H., et al., 2010. Description of the Earth system model of intermediate complexity LOVECLIM version 1.2. Geosci. Model Dev. (GMD) 3, 603–633. https://doi.org/10.5194/gmd-3-603-2010.
Graham, A.G.C., et al., 2016. Major advance of South Georgia glaciers during the Antarctic Cold Reversal following extensive sub-Antarctic glaciation. Nat. Commun. 8 https://doi.org/10.1038/ncomms14798.
Griffiths, M.L., et al., 2010. Younger Dryas–Holocene temperature and rainfall history of southern Indonesia from $\delta^{18}O$ in speleothem calcite and fluid inclusions. Earth Planet. Sci. Lett. 295, 30–36.
Grimm, E.C., Watts, W.A., Jacobson, G.L., Hansen, B.C.S., Almquist, H.R., Dieffenbacher-Krall, A.C., 2006. Evidence for warm wet Heinrich events in Florida. Quat. Sci. Rev. 25, 2197–2211.
Haug, G.H., Hughen, K.A., Sigman, D.M., Peterson, L.C., Röhl, U., 2001. Southward migration of the intertropical convergence zone through the Holocene. Science 293, 1304–1308.
He, F., et al., 2013. Northern Hemisphere forcing of Southern Hemisphere climate during the last deglaciation. Nature 494, 81–85.
Heiri, O., Brooks, S.J., Renssen, H., Bedford, A., Hazekamp, M., Ilyashuk, B., Jeffers, E.S., Lang, B., Kirilova, E., Kuiper, S., Millet, L., Samartin, S., Toth, M., Verbruggen, F., Watson, J.E., van Asch, N., Lammertsma, E., Amon, L., Birks, H.H., Birks, H.J.B., Mortensen, M.F., Hoek, W.Z., Magyari, E., Muñoz Sobrino, C., Seppä, H., Tinner, W., Tonkov, S., Veski, S., Lotter, A.F., 2014. Validation of climate model-inferred regional temperature change for late-glacial Europe. Nat. Commun. 5 https://doi.org/10.1038/ncomms5914.
Jomelli, V., et al., 2014. A major advance of tropical Andean glaciers during the Antarctic cold reversal. Nature 513, 224–228.
Mairesse, A., Goosse, H., Mathiot, P., Wanner, H., Dubinkina, S., 2013. Investigating the consistency between proxy-based reconstructions and climate models using data assimilation: a mid-Holocene case study. Clim. Past 9, 2741–2757.
Manabe, S., Stouffer, R.J., 1997. Coupled atmosphere-ocean model response to freshwater input: comparison to the Younger Dryas event. Paleoceanography 12, 321–336.
Mathiot, P., et al., 2013. Using data assimilation to investigate the causes of Southern Hemisphere high latitude cooling from 10 to 8 ka BP. Clim. Past 9, 887–901.
Mayewski, P.A., et al., 1993. The atmosphere during the younger Dryas. Science 261, 195–197.
Mellor, G.L., Yamada, T., 1982. Development of a turbulence closure model for geophysical fluid problems. Rev. Geophys. Space Phys. 20, 851–875.
Mohtadi, M., et al., 2014. North Atlantic forcing of tropical Indian Ocean climate. Nature 509, 76–80.
Monnin, E., et al., 2001. Atmospheric CO_2 concentrations over the last glacial termination. Science 291, 112–114.
Moreno, P.I., et al., 2009. Renewed glacial activity during the Antarctic cold reversal and persistence of cold conditions until 11.5 ka in southwestern Patagonia. Geology 37, 375–378.
Moreno, P.I., Videla, J., 2016. Centennial and millennial-scale hydroclimate changes in northwestern Patagonia since 16,000 yr BP. Quat. Sci. Rev. 149, 326–337.
Mudelsee, M., 2000. Ramp function regression: a tool for quantifying climate transitions. Comput. Geosci. 26, 293–307.
Muschitiello, F., et al., 2015. Fennoscandian freshwater control on Greenland hydroclimate shifts at the onset of the Younger Dryas. Nat. Commun. 6 https://doi.org/10.1038/ncomms9939.
Nikolova, I., Yin, Q., Berger, A., Singh, U.K., Karami, M.P., 2013. The last interglacial (Eemian) climate simulated by LOVECLIM and CCSM3. Clim. Past 9, 1789–1806.
Novenko, E.Y., Volkova, E.M., Nosova, N.B., Zuganova, I.S., 2009. Late glacial and Holocene landscape dynamics in the southern taiga zone of east European plain according to pollen and macrofossil records from the central forest state reserve (Valdai hills, Russia). Quat. Int. 207, 93–103.
Opsteegh, J.D., Haarsma, R.J., Selten, F.M., Kattenberg, A., 1998. ECBilt: a dynamic alternative to mixed boundary conditions in ocean models. Tellus 50, 348–367.
Partin, J.W., et al., 2015. Gradual onset and recovery of the Younger Dryas abrupt climate event in the tropics. Nat. Commun. 6 https://doi.org/10.1038/ncomms9061.
Peltier, W., 2004. Global glacial isostasy and the surface of the ice-age earth: the ICE-5G (VM2) model and GRACE. Annu. Rev. Earth Planet Sci. 32, 111–149.
Polyak, V.J., et al., 2004. Prolonged wet period in the southwestern United States through the Younger Dryas. Geology 32, 5–8. https://doi.org/10.1130/G19957.1.
Rach, O., et al., 2014. Delayed hydrological response to Greenland cooling at the onset of the Younger Dryas in western Europe. Nat. Geosci. 7, 109–112.
Rach, O., et al., 2017. A dual-biomarker approach for quantification of changes in relative humidity from sedimentary lipid D/H ratios. Clim. Past 13, 741–757.
Rasmussen, S.O., et al., 2006. A new Greenland ice core chronology for the last glacial termination. J. Geophys. Res. 111 https://doi.org/10.1029/2005JD006079.
Renssen, H., Goosse, H., Fichefet, T., Brovkin, V., Driesschaert, E., Wolk, F., 2005. Simulating the Holocene climate evolution at northern high latitudes using a coupled atmosphere-sea ice-ocean-vegetation model. Clim. Dynam. 24, 23–43.
Renssen, H., Seppä, H., Heiri, O., Roche, D.M., Goosse, H., Fichefet, T., 2009. The temporal and spatial complexity of the Holocene Thermal Maximum. Nat. Geosci. 2, 411–414. https://doi.org/10.1038/NGEO513.
Renssen, H., Mairesse, A., Goosse, H., Mathiot, P., Heiri, O., Roche, D.M., Nisancioglu, K.H., Valdes, P.J., 2015. Multiple causes of the Younger Dryas cold period. Nat. Geosci. 8, 946–949. https://doi.org/10.1038/ngeo2557.
Roche, D.M., Dokken, T.M., Goosse, H., Renssen, H., Weber, S.L., 2007. Climate of the last glacial maximum: sensitivity studies and model-data comparison with the LOVECLIM coupled model. Clim. Past 3, 205–224.
Roche, D.M., Wiersma, A.P., Renssen, H., 2010. A systematic study of the impact of freshwater pulses with respect to different geographical locations. Clim. Dynam. 34, 997–1013.
Schilt, A., et al., 2010. Atmospheric nitrous oxide during the last 140,000 years. Earth Planet Sci. Lett. 300, 33–43.
Schüpbach, S., et al., 2013. High-resolution mineral dust and sea ice proxy records from the Talos Dome ice core. Clim. Past 9, 2789–2807.
Shakun, J.D., Carlson, A.E., 2010. A global perspective on Last Glacial Maximum to Holocene climate change. Quat. Sci. Rev. 29, 1801–1816.
Shanahan, T.M., et al., 2015. The time-transgressive termination of the African humid period. Nat. Geosci. 8, 140–144.
Shi, N., et al., 2000. Correlation between vegetation in southwestern Africa and oceanic upwelling in the past 21,000 years. Quat. Res. 54, 72–80.
Spahni, R., et al., 2005. Atmospheric methane and nitrous oxide of the late Pleistocene from Antarctic ice cores. Science 310, 1317–1321.
Steffensen, J.P., Andersen, K.K., Bigler, M., Clausen, H.B., Dahl-Jensen, D., Fischer, H., Goto-Azuma, K., Hansson, M., Johnsen, S.J., Jouzel, J., Masson-Delmotte, V., Popp, T., Rasmussen, S.O., Röthlisberger, R., Ruth, U., Stauffer, B., Siggaard-Andersen, M.-., Sveinbjörnsdóttir, Á.E., Svensson, A., White, J.W.C., 2008. High-resolution Greenland ice core data show abrupt climate change happens in few years. Science 321, 680–684.
Stouffer, R.J., et al., 2006. Investigating the causes of the response of the thermohaline circulation to past and future climate changes. J. Clim. 19, 1365–1387.
Subetto, D.A., et al., 2002. Climate and environment on the Karelian Isthmus, northwestern Russia, 13000–9000 cal. yrs BP. Boreas 31, 1–19.
Talbot, M.R., Filippi, M.L., Jensen, N.B., Tiercelin, J.-J., 2007. An abrupt change in the African monsoon at the end of the Younger Dryas. G-cubed 8. https://doi.org/

10.1029/2006GC001465. Q03005.
Timmermann, A., Justino Barbosa, F., Jin, F.F., Goosse, H., 2004. Surface temperature control in the North Pacific during the last glacial maximum. Clim. Dynam. 23, 353–370. https://doi.org/10.1007/s00382-004-0434-9.
Van Meerbeeck, C.J., Renssen, H., Roche, D.M., 2009. How did marine isotope stage 3 and last glacial maximum climates differ? Perspectives from equilibrium simulations. Clim. Past 5, 33–52.
Voelker, S.L., et al., 2015. Deglacial hydroclimate of midcontinental North America. Quat. Res. 83, 336–344.
Wagner, J.D.M., et al., 2010. Moisture variability in the southwestern United States linked to abrupt glacial climate change. Nat. Geosci. 3, 110–113.
Wang, Y.J., et al., 2001. A high-resolution absolute-Dated late pleistocene monsoon record from hulu cave, China. Science 294, 2345–2348.
Wohlfarth, B., et al., 2002. Late-glacial and early Holocene environmental and climatic change at lake tambichozero, southeastern Russian karelia. Quat. Res. 58, 261–272.
Yin, Q.Z., Berger, A., 2012. Individual contribution of insolation and CO_2 to the interglacial climates of the past 800,000 years. Clim. Dynam. 38, 709–724. https://doi.org/10.1007/s00382-011-1013-5.